RTK Feasibility Analysis for GNSS Snapshot Positioning

Xiao Liu[1, 2], Miguel Ángel Ribot[1], Adrià Gusi-Amigó[1], Pau Closas[1, 3], Adrià Rovira Garcia[2], and Jaume Sanz Subirana[2]

[1]Albora Technologies
[2]Research group of Astronomy and GEomatics (gAGE), Universitat Politècnica de Catalunya (UPC)
[3]Electrical, and Computer Engineering Dept., Northeastern University, Boston MA

BIOGRAPHIES

Mr. Xiao Liu got his MS degree in GNSS from École Nationale de l'Aviation Civile (ENAC), Toulouse, France. Currently, he is completing his industrial PhD program at Albora Technologies in cooperation with Universitat Politècnica de Catalunya (UPC). His research interests include Differential GNSS data processing, snapshot GNSS and related applications for IoT and Autonomous Vehicles.

Dr. Miguel Ángel Ribot is co-head of the GNSS team at Albora Technologies, in Barcelona, Spain. He received his B.Sc. in Electrical Engineering from Universitat de les Illes Balears in 2008, his M.Sc. in Information and Communication Technologies from the Universitat Politècnica de Catalunya (UPC) in 2011, and his Ph.D. from the École Polythecnique Fédérale de Lausane (EPFL) in 2017. His research interests include statistical and array signal processing, estimation and detection theory, remote sensing, and GNSS receiver design for precise and robust navigation.

Dr. Adrià Gusi-Amigó is co-head of the GNSS team at Albora Technologies, Barcelona, Spain. He received the M.Sc in Electrical Engineering from the Universitat Politècnica de Catalunya in 2010, and the PhD in Electrical Engineering from the Université Catholique de Louvain in 2015. His main research interests include signal processing for ranging and positioning, multiuser and multipath interference, and analysis of estimation lower bounds.

Prof. Pau Closas is Assistant Professor at Northeastern University, Boston, MA. He received the MS and PhD degrees in Electrical Engineering from UPC in 2003 and 2009. He also holds a MS in Advanced Mathematics from UPC, 2014. His primary areas of interest include statistical signal processing, robust stochastic filtering, and machine learning, with applications to positioning systems and wireless communications. He is the recipient of the 2014 EURASIP Best PhD Thesis Award, the 9th Duran Farell Award, the 2016 ION Early Achievements Award, and a 2019 NSF CAREER Award.

Dr. Adrià Rovira Garcia is a Serra Hunter Fellow with the Department of Physics (UPC) and member of gAGE since 2009. He co-authors 15 papers in peer-reviewed journals, two book chapters and over 25 works in meeting proceedings, with one best presentation award from the US Institute of Navigation. His research interests are focused on high accuracy navigation under scintillation

Prof. Dr. Jaume Sanz Subirana is with the Department of Mathematics (UPC) and co-founder of gAGE/UPC research group in 1987. He has published over 70 papers in peer-reviewed journals, more than 200 works in meeting proceedings related with GNSS. He is a co-author of five patents on GNSS and four books on GNSS Data Processing. He is Membership of the GNSS Scientific Advisory Group (GSAC) of the European Space Agency (ESA).

ABSTRACT

With snapshot positioning becoming popular for various applications, the present contribution focuses on the feasibility of achieving Real Time Kinematics (RTK) positioning using snapshot data, i.e. a very brief interval of the received satellite signal. This method is termed as Snapshot RTK (SRTK). We first introduce the general workflow of snapshot positioning and the SRTK engine functioning blocks. Their differences from traditional receivers and challenges brought by the short duration of data are explained. Since a major difference of this positioning method is the generation of code and carrier-phase GNSS observables, we go through this procedure in details. In order to explore the feasibility of achieving RTK under different scenarios, the rate of Integer Ambiguity Resolution (IAR) is assessed by using snapshot measurements generated with different integration times and signal bandwidths under zero-baseline configuration. Under these assumptions, the key factor that influences the RTK fix rate is the code measurement noise. Double Difference (DD) code measurement errors are evaluated and plotted together with the resulting IAR fix rates in order to find the relationship between them. The performance of using multi-constellation and multi-frequency signals is tested as well. The fix rate can reach 100% when multiple constellations are used. The achieved positioning accuracy is shown to be less than 5 mm in horizontal domain when IAR is achieved successfully. Finally, some conclusions and thoughts about future research steps on SRTK are given.

INTRODUCTION

Global Navigation Satellite System (GNSS) receivers play an important role in the applications such as Internet-of-Things (IoT) and Location-Based-Services (LBS) [1–3]. These services usually have a large amount of users and that is why positioning service providers choose receivers that not only provide accurate navigation solutions, but also have a low cost and power consumption. The trade-off between accuracy, cost and power consumption is critical for the service providers. Among all the new GNSS methods, a very promising concept is the cloud-based receiver [4]. This type of receiver takes a snapshot of data recorded by a radio front-end and transmits it to the cloud, where all the following signal and data processing are executed. The cloud platform has the advantage of powerful computational capability and benefits from the convenience of online assistance data such as precise satellite ephemeris and atmosphere correction models. Applications like asset tracking are ideal for this type of receivers as they request position information only at the epochs when the users need to find the device, during the rest of the time, the receiver can be switched to sleep mode in order to save power. Cloud-based snapshot receivers have a higher efficiency than conventional receivers in terms of energy consumption [5].

Operating with short data recordings requires a different architecture of signal processing engine. Currently, most commercial GNSS receivers follow a traditional close-loop scheme. That is, tracking the received signal and then generating code-pseudorange and carrier phase measurements, which are finally used as input to compute the navigation solutions. Snapshot receivers, however, implementing open-loop architectures, require external assistance and a modified navigation filter to compute a position fix [6] [7].

The positioning accuracy depends on the satellite geometry and the quality of code pseudorange and carrier phase measurements. The former is only influenced by the number and position of satellites in view, whereas the latter can be influenced by the environment and receiver settings such as integration time, signal bandwidth, etc. Since cloud platform has the natural advantage of access to online differential correction data to cancel out common errors from orbit, satellite clock, and propagation effects, the main concern for snapshot receivers is the measurement noise. In addition, Real Time Kinematics (RTK) reaches centimeter level accuracy when the carrier phase Integer Ambiguity Resolution (IAR) can be performed successfully, although it requires high quality of code and carrier phase measurements. This concept of achieving instant RTK fix is what we refer to as Snapshot RTK (SRTK). In order to achieve SRTK, a few challenges have to be tackled. On the one hand, the values of the unkown phase ambiguities are changing for every epoch, which can be understood as if all carrier phase measurements present a cycle slip. This requires a high efficient algorithm to achieve IAR instantly. The Least-squares AMbiguity Decorrelation Adjustment (LAMBDA) Integer Least Square (ILS) algorithm [8] is a good example as it has the best performance compared to other IAR algorithms [9]. On the other hand, the fact that snapshot receivers only produce fractional carrier phase measurements makes IAR more difficult. In addition, the generation of code and carrier phase observables is totally different from traditional GNSS receivers as snapshot data are usually too short to decode time information. While [10] shows that SRTK fix is achievable under certain Signal to Noise Ratio (SNR) requirements, these conclusions are based on simulated data, which avoids most bothersome influences from actual environments.

The aim

We define the RTK feasibility as the IAR fix rate in this paper. The aim of the present contribution is to achieve RTK IAR using real snapshot recordings. Based on that, we further analyze the IAR fix rates and explore the necessary conditions in order to obtain a RTK fixed solution in a single epoch. SRTK experiments with different settings of signal bandwidth and integration time are performed in order to characterise their influences on the fix rate. Besides, Double Difference (DD) code measurement error magnitudes are investigated and their relationship with the IAR fix rates is another target to be explored in this paper.

Paper structure

The paper is organised as follows. The present section is the Introduction. In the next section, we introduce the theoretic background about SRTK, methods used to generate snapshot measurements, and the navigation filter details. Then, in the third section, we explain the experiments setup for all the data collected for this paper. In section 4 "Results and discussions", the SRTK processing results of these data are analysed and discussed. Finally, the conclusions about SRTK feasibility are drawn in the last section.

METHODOLOGY: SRTK MEASUREMENTS AND FILTER

This section first introduces the general work flow of snapshot positioning and the navigation engine of SRTK. The processing details about the generation of GNSS measurements are then described. This is followed by the explanations of the equations used in the navigation filter for SRTK.

SRTK Workflow

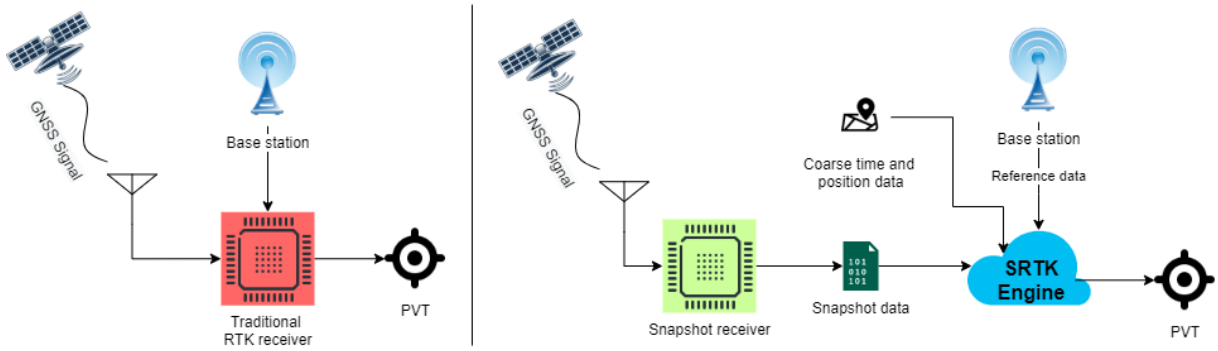

Figure 1: Comparison of traditional RTK receiver workflow (left) and SRTK workflow (right).

Figure 1 illustrates the basic architectures of two types of GNSS receivers. The cloud-based SRTK receiver is depicted on the right side. It starts from the snapshot receiver receiving the GNSS signal from the antenna and down converting it to base band. Then, it relies on a communication module to transmit the collected snapshot data to the cloud. Meanwhile, the cloud platform gathers all the necessary data to support the SRTK processing, the assistance data include a rough estimate of time and position of the user, the ephemeris data and base station observables, etc. Then, all the signal and data processing, as part of the SRTK engine, is processed on the cloud. The output Position Velocity and Time (PVT) solution is then fed to the client user front end, such as an asset tracking web page, or sent back to the receiver depending on the user needs. This solution may be stored to be used as the rough position input for the future snapshots generated on the same receiver. As a comparison, a traditional RTK receiver workflow is depicted on the left side of Figure 1. The main difference is that traditional RTK receivers have the whole positioning engine located on the receiver while snapshot receivers have the processing in the cloud, which leaves the GNSS hardware as simple as a radio front-end. For this reason snapshot receivers have a much smaller energy demand compared to traditional receivers [11].
The blocks composing the SRTK engine are illustrated in Figure 2. The incoming signal samples first pass through an assisted acquisition module that generates time delay, Doppler frequency and carrier phase measurements referenced

to the beginning of the snapshot. Then, together with assistance data of rough position and time of the user, the time delay and Doppler measurements go through a Coarse-time navigation filter as described in [12] in order to solve the receiver time millisecond ambiguities. With this process we obtain an estimate of the receiver time and position. These results are then used to generate a RINEX file which is later used in the RTK navigation filter together with the base station observation data. Finally, the SRTK engine outputs a RTK PVT solution. More details about the SRTK engine functional blocks of are described below.

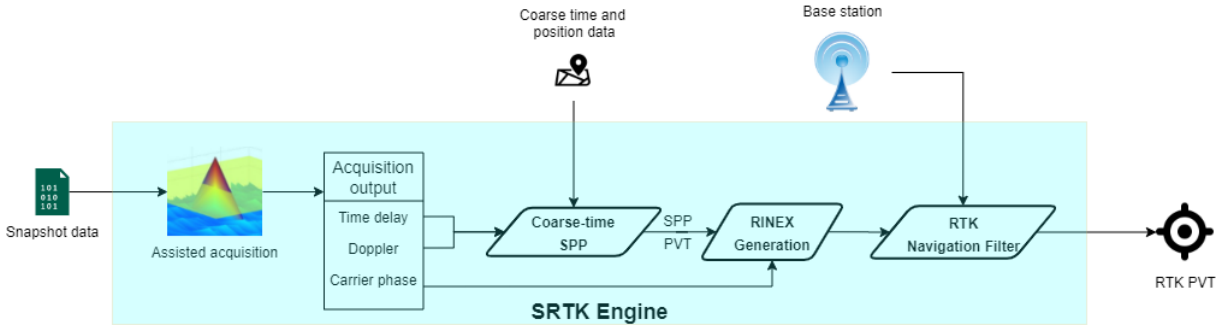

Figure 2: Internal architecture of SRTK engine.

Pseudorange and carrier phase generation

In a traditional receiver, a satellite acquisition process is adopted to detect the coarse code phase and Doppler frequency of the received signal, after that, tracking loops such as Delay Lock Loop (DLL) and Phase Lock Loop (PLL) are applied to generate precise measurements. However, this is not possible for snapshot receivers due to the limitation of short period of snapshot data. An open-loop architecture has to be implemented for snapshot receivers. The time delay estimation is done by exploiting the auto-correlation properties of the Pseudo-Random Noise (PRN) codes. In order to estimate the delay of the signal with a greater accuracy, the use of interpolation techniques is necessary [7]. Similarly for Doppler measurements, a narrow-bin search and a interpolation method is used in order to obtain a high precision on this measurement. The carrier phase measurement is generated by exploiting the phase of the complex Inverse Fast Fourier Transform (IFFT) output. The obtained carrier phase measurement is a fractional value between 0 and 2π since no accumulation steps are applied like in close-loop methods. In order to increase the speed of this processing, assistance data are used to reduce the number of choice bins of Doppler and Code delays. Some further data processing steps are necessary after these measurements are obtained by the acquisition step.
While the code delays only represent the distance from the start of the received signal samples to the beginning of the code period in GPS time, the receiver must build the full pseudoranges to make it work with standard in a navigation filter. Fortunately, with the assistance data from the cloud, we can assign different numbers of integer code periods based on the geometric ranges of the satellites to form the full pseudoranges, same as how the millisecond ambiguities are resolved in the coarse-time SPP filter [12].
As for carrier phase measurements, while adding integers to these phase measurements does not influence the RTK filter as the integers are estimated as part of the unknowns, when generating RINEX files, it is advised to pre-align an integer that correspond to the magnitude of code pseudoranges to the phase in order to avoid any numerical issues that might occur in the positioning engines. Besides, many positioning engines have the option to detect cycle slips before processing the data. It is important to disable this feature if it blocks the data from being processed, simply because using snapshot data means every epoch has a cycle slip, or as [13] explained in a more positive way, SRTK is immune to carrier-phase cycle slips since the aim is to achieve IAR in a single epoch.
As an intermediate product of snapshot RTK, a snapshot RINEX file can be generated by gathering all the measurements, so that it can fit different positioning engines in order to compute a PVT solution. Besides, with these data collected in a file, they can be processed in post-processing mode as well.

SRTK navigation filter

For the SRTK navigation filter, the implementation is not much different from other softwares such as RTKLIB [14]. In order to achieve IAR, the typical three-step procedure is adopted [15]. These three steps are, namely, calculation

of float solution, DD ambiguity integer estimation and re-calculation of fixed solution are explained hereafter.
First of all, the float solutions are calculated based on both code and phase measurements. For this step, a simple single-epoch Weighted Least Square (WLS) is applied instead of the more conventional Kalman filter that makes use of time-history information. The DD code and phase measurement pre-fit residuals are the inputs of the WLS. These pre-fit residuals are calculated by subtracting geometric range of the receiver and all modeling terms from the measured pseudoranges [16]. For zero-baseline configuration, we can safely consider that measurement errors caused by atmosphere, clocks and ephemeris cancel out in the DD process [17], yielding the following equations of DD phase and code:

$$\begin{aligned} \Phi_{rb,i}^{jk} &= \rho_{rb}^{jk} + \lambda_i \left(b_{rb,i}^{j} - b_{rb,i}^{k} \right) + \varepsilon_\Phi \\ P_{rb,i}^{jk} &= \rho_{rb}^{jk} + \varepsilon_P \end{aligned} \tag{1}$$

In this equation, $\Phi_{rb,i}^{jk}$ and $P_{rb,i}^{jk}$ are the DD pre-fit residuals of the carrier phase and pseudorange measurements. The subscript r and b stand for rover and base respectively while the superscript j and k are the indices for the two satellites used to build this DD measurement. ρ_{rb}^{jk} stands for the DD geometric range. The term $b_{rb,i}^{j}$ represents the Single Difference (SD) ambiguity between the rover and base receivers and λ_i is the wavelength for frequency i.
Notice that for phase measurements, the DD ambiguity terms are represented by the subtraction of SD ambiguities, as the SD ambiguities $\boldsymbol{b}_i = \left(b_{rb,i}^{1}, b_{rb,i}^{2}, \ldots, b_{rb,i}^{m} \right)^T$ are estimated in the filter instead of the DD values in order to simplify the reference satellites re-selection process. Here the superscript m represents the number of satellites used in the filter. Besides these SD ambiguities, the baseline vector $\boldsymbol{r}_r$ holds the remaining unknowns included in the WLS states:

$$\mathbf{x} = \left(\boldsymbol{r}_{\boldsymbol{r}}^T, \boldsymbol{b}_{\boldsymbol{i}}^T \right)^T \tag{2}$$

Within a total of m satellites, index 1 is considered as the reference satellite, then we can construct the measurements and corresponding geometry matrix as:

$$\mathbf{y} = (\Phi_{rb,i}^{12}, \Phi_{rb,i}^{13}, \ldots, \Phi_{rb,i}^{1m}, P_{rb,i}^{12}, P_{rb,i}^{13}, \ldots, P_{rb,i}^{1m})^T \tag{3}$$

$$\mathbf{H} = \begin{pmatrix} \mathbf{D} \cdot \mathbf{U_b} & \mathbf{D} \\ \mathbf{D} \cdot \mathbf{U_b} & \mathbf{0} \end{pmatrix} \tag{4}$$

Where the term $\mathbf{U}_b = \left(\mathbf{e}_b^1, \mathbf{e}_b^2, \ldots, \mathbf{e}_b^m \right)^T$ represents the Line-of-Sight (LoS) vector for all satellites calculated at the base receiver position. Here $\mathbf{e_b^j}$ is the unit vector from the base to satellite j. Matrix $\mathbf{D}$ is used to conduct the differencing procedure among satellites. It can be expressed as:

$$\mathbf{D} = \begin{pmatrix} 1 & -1 & 0 & \cdots & 0 \\ 1 & 0 & -1 & \cdots & 0 \\ \vdots & \vdots & \vdots & \ddots & \vdots \\ 1 & 0 & 0 & \cdots & -1 \end{pmatrix} \tag{5}$$

Note that the column of **1**s may change position depends on the index of the selected reference satellite. The float solutions and covariance matrix of the output unknowns are then calculated using:

$$\hat{\mathbf{x}} = \mathbf{x}_0 + \left(\mathbf{H}^T \mathbf{W} \mathbf{H} \right)^{-1} \mathbf{H}^T \mathbf{W} \mathbf{y} = \left(\hat{\boldsymbol{r}}_r^T, \hat{\boldsymbol{b}_i}^T \right)^T \tag{6}$$

$$\mathbf{P}_{\hat{\boldsymbol{x}}} = \left(\mathbf{H}^T \mathbf{W} \mathbf{H} \right)^{-1} = \begin{pmatrix} \mathbf{P}_{\hat{\boldsymbol{r}}_r} & \mathbf{0} \\ \mathbf{0} & \mathbf{P}_{\hat{\boldsymbol{b}}_i} \end{pmatrix} \tag{7}$$

$\mathbf{x}_0$ is the initial estimate of the baseline and SD ambiguity vector, in this paper a zero vector is applied as we use the base station coordinates as the initial guess of rover position. The weighting matrix $\mathbf{W}$ is constructed that the phase measurements have 300 times higher weight than that of the code measurements, due to the fact that phase measurements are much more precise. The output gives us the estimated DD ambiguities by $\mathbf{D}\hat{\boldsymbol{b}_i}$, and its covariance matrix as $\mathbf{D}\mathbf{P}_{\hat{\boldsymbol{b}}_i}\mathbf{D}^T$.

These outputs are then fed to the second step of IAR: Integer estimation. The LAMBDA ILS method is adopted in this paper as it has been proved an efficient method of integer estimation [9]. After the proper integers are

determined, the last step is to use them back in equation 1 to obtain a fixed solution with high accuracy thanks to the now unambiguous phase measurements.
Besides providing the best estimate of the integer ambiguities, the LAMBDA method also provides the second best candidate ambiguity vector and calculates their distances to the float ambiguity vector in the metric of the variance-covariance matrix. The ratio between these two distances is used as an indicator about the reliability of the output ambiguity integers and based on that a simple "Ratio-Test" can be implemented. This ratio factor is named as the LAMBDA Ratio Factor (LRF) in the following discussions. A LRF value of 3 is used in this paper as the threshold to determine if the solution is fixed. The IAR fix rate is calculated as the percentage of snapshots with LRF greater than this threshold. The fix rate is used as the main parameter to indicate the RTK feasibility.

EXPERIMENT GOALS AND SETUP

In order to experiment on the feasibility of SRTK IAR under different conditions, several sets of data have been generated and analysed. The original rover data were collected by a Labsat GNSS signal recorder [18] with signals from L1 and L5 frequency bands at 58 MHz sampling rate with a bandwidth of 56 MHz. The reference station data was collected by a Septentrio PolaRx-5e receiver connected to a PolaNt-x Multi Frequency antenna that is statically located on a roof near Barcelona, Spain, as can be seen in Figure 3. In order to avoid the influences from other

Figure 3: Antenna location

measurement errors, in this paper we use RTK in "zero-baseline" configuration. For that the Labsat and the base receiver are connected to the antenna through a splitter that ensures the same signal is received by them. Besides, a satellite elevation cut-off angle has been set at 10 degrees. The total length of the rover data recording is 90 seconds, collected on 19th of May, 2020. We have divided this data set into 450 snapshots with each snapshot having a length of 200 ms. The Septentrio receiver started recording base station files 5 minutes before the Labsat started recording to ensure that the rover snapshots can get a timely correction data for SRTK. The base station provides measurements at a 1 Hz rate.
In this paper, the following 3 terms have been investigated:

1. Influence of integration time and bandwidth on IAR fix rate
2. Relationship of code noise level and IAR fix rate
3. Influences of multi-constellation and multi-frequency data on IAR fix rate

The following experiments are set up with these goals in mind. First of all, in order to evaluate the RTK fix rate using different integration times. We have run the SRTK filter with integration times of 20 ms, 40 ms, 60 ms, 80 ms and 100 ms, while keeping all other settings identical for these executions. For evaluating the influence of different bandwidths, we have down-sampled the original 58 MHz files to lower values, since reducing sampling frequency also effectively reduces the bandwidth as well. We have obtained data sets with bandwidths of 11.2 MHz, 14 MHz, 15.4 MHz, 17.5 MHz, 19.6 MHz, and 24.5 MHz. Signals from GPS L1CA are used here for the analysis.
For the second goal, the DD code measurements are also saved before being fed to the WLS calculation while running

SRTK, from that we can calculate the DD code measurement Root Mean Square Error (RMSE) from all satellites for each epoch of the data sets, with the following expression:

$$RMSE(n) = \sqrt{\sum_{j=2}^{m} (P_{rb,i}^{1j}(n))^2/(m-1)} \tag{8}$$

Where n represents the index for the snapshot epoch. Same as before, j is the satellite index, and m is the total number of satellites used. The first satellite is used as the reference satellite and that's why the summation starts with $j = 2$. With these data in hand, we can infer the relationship between the SRTK fix rate and the DD code measurements noise level.
Besides the code noise, the use of other constellations also influences the final IAR fix rate. As the number of satellites increases when multi-constellation signals are used, this influences the precision of the estimated float ambiguities, and thus impact the fix rate. For the third goal, both GPS and Galileo constellations are used for multi-constellation processing while L1 and L5 frequency bands are applied for multi-frequency processing. The resulted solutions are then compared with the single constellation single frequency solutions in terms of RTK fix rate.

RESULTS AND DISCUSSIONS

Integration time and bandwidth impact

First of all, the variation of calculated LRF and DD code measurement RMSE are represented in the time domain. As an example, outputs for data set of 11.2 MHz bandwidth with different integration times are shown in Figure 4. Only GPS L1CA signal is used for this processing, and the carrier-to-noise density (C/N_0) values of these satellites are plotted in Figure 5.

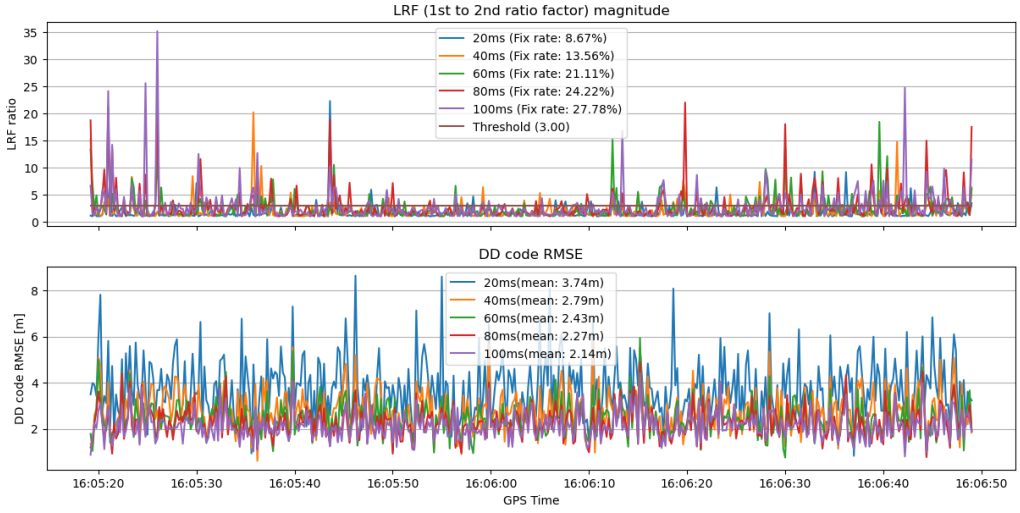

Figure 4: Time plot of LRF and DD code RMSE for 11.2 MHz bandwidth

As can be seen in the top panel of Figure 4, the LRF appears to be quite noisy along time since SRTK engine takes one snapshot data a time and these data are totally independent from other epochs. The DD code RMSE is calculated based on all satellites from only the current snapshot of data, thus it is noise-like as well, as depicted in the bottom panel of Figure 4. However, as expected, the mean magnitude of this parameter decreases when longer integration time is used, which means the rover code measurement quality has improved. The blue curve, which represents the signal with integration time of 20 ms, shows a larger DD code RMSE compared to the purple curve that represents an integration time of 100 ms. To show this trend more clearly, Figure 6 shows this pattern on the right panel using data with other bandwidths as well.
It can be observed in Figure 6 on the left that the IAR fix rate increases when the integration time increases. However,

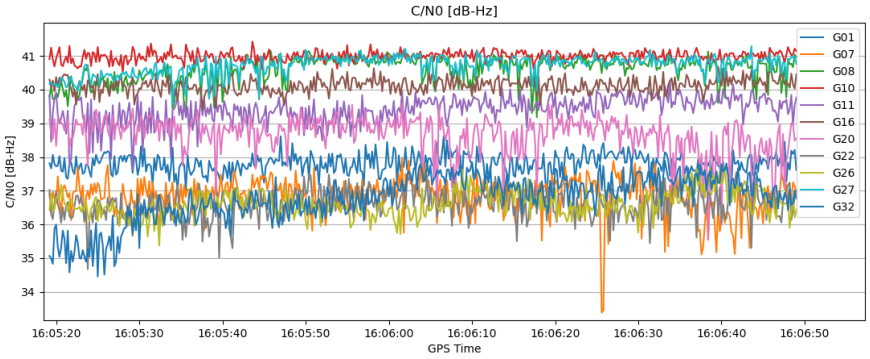

Figure 5: C/N_0 of GPS satellites in the collected data

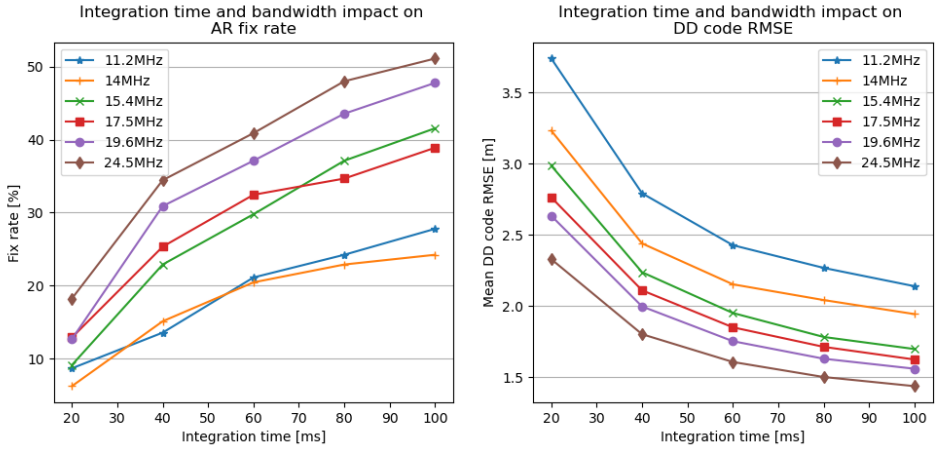

Figure 6: Integration time and bandwidth impact on fix rate and DD code RMSE

with only GPS L1CA signal used, the best RTK fix rate achieved in these experiments is only 51%. When 20 ms of integration time is used, the fix rate are all below 20%. The plot on the right shows that the longer integration time we use, the lower DD code measurement RMSE we can get. Note that for this plot, the RMSE are calculated based on all the epochs of this data set. The lowest DD code RMSE value obtained in these date sets is less than 1.5 m, which corresponds to the fix rate of 51%. While looking at the curves from different signal bandwidth, it is concluded that the fix rate and code measurement quality both improve when the signal has a larger bandwidth.

Code noise impact

Same as the previous subsection, in order to explore the code noise impact, GPS L1CA signals with the 5 different integration time and 6 different bandwidth settings mentioned in previous section are applied, which means a total of 30 sets of measurements are available for the code quality impact analysis, with 450 epochs included in each of them. The DD code RMSEs of all satellites are calculated for each of these 13500 snapshots. The results are plotted in Figure 7 on the left. There is a pattern that with smaller DD code RMSE, the LRF tends to be higher and thus result in a higher fix rate. In order to show the relationship between the DD code quality and the fix rate, a simple partitioning is performed. We sort these data points by their DD code RMSE magnitudes in an ascending order and divide them into 270 groups with the sorted index, each group has 50 snapshots and the maximum DD code RMSE of the current group is smaller than the minimum of the next group. The mean LRF and fix rate of each group is calculated and plotted on the right side of Figure 7.
The trend matches the raw data points on the left, which shows a decrease in fix rate and mean LRF when the code RMSE goes higher. From this plot we can also see that in order to achieve a 90% fix rate, we should have DD code

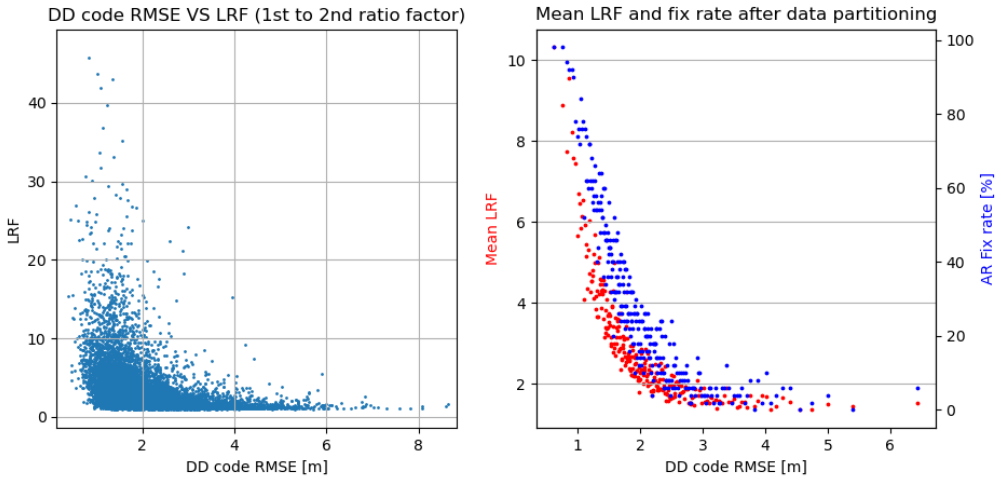

Figure 7: Relation ship between DD code RMSE, IAR fix rate and LRF

measurement RMSE smaller than 1 m, which correspond to a mean LRF between 6 and 8.

Multi-constellation and multi-frequency impact

To investigate the improvements brought by using Multi-Constellation Multi-Frequency (MCMF) signals, different combinations are considered as shown in Table 1. Same as in previous sections, signals of 6 different bandwidths are processed while other settings are kept identical for all these scenarios. The integration time is set to 100 ms for this experiment.

Bandwidth [MHz]	GPS L1CA	GAL E1C	GAL E5A	GPS L1CA& GAL E1C	GPS L1CA& GPS L5	GAL E1C& GAL E5A	MCMF
11.2	27.78%	36.67%	23.56%	100%	97.33%	100%	100%
14	24.22%	43.11%	69.78%	100%	98.67%	100%	100%
15.4	41.56%	45.33%	90.89%	100%	99.78%	100%	100%
17.5	39.11%	50%	99.56%	100%	99.78%	100%	100%
19.6	48%	50.22%	100%	100%	100%	100%	100%
24.5	51.33%	57.33%	100%	100%	100%	100%	100%

Table 1: IAR rate with different combinations of constellation and frequency bands, with 100 ms integration time

When only using GPS L1CA signals, the maximum fix rate that can be reached among all these data sets is 51.33%, it is slightly higher when using Galileo E1C only, although the maximum fix rate is still only 57.33%, which is achieved at the bandwidth of 24.5 MHz. However, Galileo E5A signal brings an improvement in terms of fix rate, except for the cases when a bandwidth of 11.2 MHz is used, in other cases of bandwidths of 19.6 MHz and 24.5 MHz, the fix rates are 100%. Note that the nominal bandwidth of Galileo E5A signal is 20 MHz, it can be expected that their performance is worse when a lower bandwidth is used. The case with GPS L5 signal only is not listed here because there are only 5 GPS satellites observed in this data set transmitting signals in L5 frequency band, and no IAR fix has been achieved for this case. However, When both GPS and Galileo constellations are used, the result shows that IAR is not a problem anymore, as a 100% fix rate is obtained for all these scenarios. As for multi-frequency processing, the output fix rate is also almost 100% for all scenarios, except for the cases when GPS L1CA and L5 are used with bandwidths lower than 17.5 MHz, nevertheless, these values are still higher than 97%. The column for MCMF represents that case when all four signals are used, and 100% fix rate can be achieved as well in this case.

Positioning accuracy

When IAR has been achieved, centimeter level accuracy is expected from the fixed solutions. The positioning results when using GPS L1CA and GPS L5 signal at 24.5 MHz bandwidth is presented in Figure 8. The positioning errors

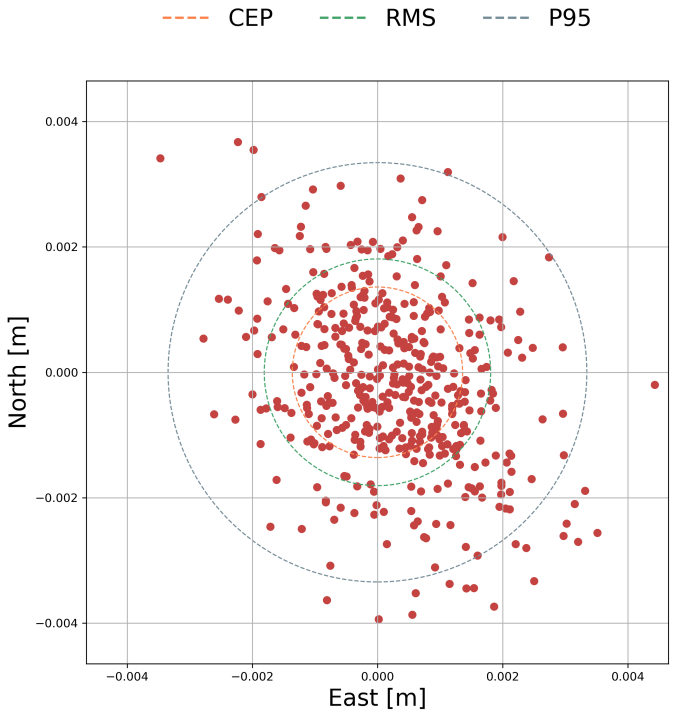

Figure 8: SRTK fixed solution accuracy

in north and east are all less than 5 mm. The Circular Error Probable (CEP) circle, shown in orange color, contains half of the positioning points inside, and it has a radius of 1.4 mm. The RMSE in the horizontal domain is presented as the green circle and has a magnitude of 1.8 mm. The P95 circle, which represents the error magnitude that 95% of the data points can reside in, has a radius of 3.4 mm. Note that these results correspond to a zero baseline experiment with a high-end reference receiver. Overall this positioning accuracy is extremely high and should satisfy any IoT or LBS applications.

CONCLUSIONS

The main goal of this paper is to demonstrate the feasibility of SRTK using real signals under different scenarios in terms of integration time and signal bandwidth. This has been achieved as IAR can be performed successfully. To the best of our knowledge, this is the first time that SRTK has been achieved with live signal recordings. The real data results have shown that SRTK is feasible as long as the noise of the code measurements remains low. More specifically, a DD code RMSE of all satellites lower than 1 m allows a fix rate higher than 90%. Increasing the integration time used in the assisted acquisition step improves the code measurements quality and as a result, increases the IAR fix rate. The same goes for the bandwidth parameter, the higher it is, the more possible the ambiguities can be fixed. Besides, as shown in the results, when considering the processing from independent constellations, Galileo signals perform slightly better than GPS signals, while using multiple constellations together has totally solved this problem. A 100% fix rate is achieved for all the data sets that have been used in multi-constellation mode. Using L1 and L5 frequencies together also dramatically increases the fix rate, it has a performance of over 97% fix rate for all bandwidths used. In contrast, the fixed rate is lower than 60% when single frequency is used. After the ambiguities are fixed, the positioning solution under zero-baseline configuration is accurate to millimeter level, the errors in horizontal domain are all smaller than 5 mm.

As research on SRTK is still at the preliminary stage, it is an innovative field that a lot more aspects can be investigated in the future. The data processed in this paper is very limited and further experiments shall confirm this findings. One important aspect to investigate is the relationship between the baseline distance and the fix rate, this is especially important for practical applications. Besides, influences from atmosphere, multi-path, maximum delay of correction data can all influence the feasibility of SRTK and need to be further investigated.

ACKNOWLEDGEMENTS

The author would like to acknowledge Albora Technologies for the technical support during the whole course of this research, including collection of raw data and developments of related software and libraries. The authors would like to thank Everis Aeroespacial y Defensa, S.L.U. for lending the Septentrio base station receiver for this research. The research reported in this paper has been partially supported by the Doctorat Industrial Grant 2018 DI 082 from the Generalitat de Catalunya, and the Spanish Ministry of Science, Innovation and Universities project RTI2018-094295-B-I00. P. Closas was partially supported by the National Science Foundation under Awards CNS-1815349 and ECCS-1845833.

REFERENCES

[1] European GNSS Agency (GSA), *GNSS market report*, Publications Office of the European Union, Luxembourg, Oct. 2019.

[2] Davide Dardari, Marco Luise, and Emanuela Falletti, *Satellite and Terrestrial Radio Positioning Techniques: A Signal Processing Perspective*, Academic Press, 2011.

[3] Davide Dardari, Pau Closas, and Petar M Djurić, "Indoor tracking: Theory, methods, and technologies," *IEEE Transactions on Vehicular Technology*, vol. 64, no. 4, pp. 1263–1278, 2015.

[4] Keith Van Dierendonck and Ossama Al-Fanek, "What is snapshot positioning and what advantages does it offer?," Dec 2018.

[5] V. Lucas-Sabola, G. Seco-Granados, J.a. Lopez-Salcedo, J.a. Garcia-Molina, and M. Crisci, "Efficiency analysis of cloud gnss signal processing for iot applications," *Proceedings of the 30th International Technical Meeting of The Satellite Division of the Institute of Navigation (ION GNSS 2017)*, Mar 2017.

[6] D. Jiménez-Baños, N. Blanco-Delgado, G. López-Risueño, G. Seco-Granados, and A. Garcia-Rodríguez, "Innovative Techniques for GPS Indoor Positioning Using a Snapshot Receiver," *Proceedings of the 19th International Technical Meeting of the Satellite Division of The Institute of Navigation (ION GNSS 2006)*, pp. 2944–2955, September 2006.

[7] Nicola Linty, "Snapshot estimation algorithms for GNSS mass-market receivers," *PhD dissertation. Politecnico Di Torino, Torino, Italy*, Apr. 2015.

[8] P. Teunissen, "The least-squares ambiguity decorrelation adjustment: A method for fast GPS integer ambiguity estimation," *Journal of Geodesy*, vol. 70, pp. 65–82, 11 1995.

[9] P. Teunissen, P. Joosten, and C. Tiberius, "A Comparison of TCAR, CIR and LAMBDA GNSS Ambiguity Resolution," in *Proceedings of ION GPS 2002*, Portland, Oregon, USA, Sept. 2002, pp. 2799–2808.

[10] Daniel Medina, Lorenzo Ortega, Jordi Vila-Valls, Pau Closas, Francois Vincent, and Eric Chaumette, "A new compact CRB for delay, doppler and phase estimation - application to GNSS SPP & RTK performance characterization," *IET Radar, Sonar Navigation*, June 2020.

[11] European GNSS Agency (GSA), *Power-efficient positioning for the Internet of Things*, Publications Office of the European Union, Luxembourg, June 2020.

[12] Frank Van Diggelen, *A-GPS: Assisted GPS, GNSS and SBAS*, chapter 4, pp. 61–102, Artech House, 2009.

[13] Kan Wang, Pei Chen, and Peter Teunissen, "Single-epoch, single-frequency multi-GNSS L5 RTK under high-elevation masking," *Sensors*, vol. 19, no. 5, pp. 1066, Mar 2019.

[14] T. Takasu, "RTKLIB: Open Source Program Package for RTK-GPS," in *Free and Open Source Software for Geospatial Conference*, Tokyo, Japan, Nov. 2009.

[15] P. Teunissen, P. de Jonge, and C. Tiberius, "The LAMBDA method for fast GPS surveying," in *Proceedings of the International Symposium GPS Technology Applications*, Bucharest, Romania, Sept. 1995, pp. 203–210.

[16] J. Sanz Subirana, J.M. Juan Zornoza, and M. Hernández-Pajares, *GNSS DATA PROCESSING, Volume I: Fundamentals and Algorithms*, vol. 1, ESA Communications, ESTEC, PO Box 299, 2200 AG Noordwijk, the Netherlands, May 2013.

[17] Andre Hauschild, "Combinations of observations," in *Springer Handbook of Global Navigation Satellite Systems*, Peter J.G. Teunissen and Oliver Montenbruck, Eds., chapter 20, pp. 599–601. Springer International Publishing, 2017.

[18] "LabSat 3 Wideband. https://www.labsat.co.uk/index.php/en/products/labsat-3-wideband," 2019.